JOURNAL OF CATALYSIS 173, 53–63 (1998)
ARTICLE NO. CA971889

# Theoretical Study on the Decomposition of HCOOH on a ZnO(10$\bar{1}$0) Surface

Masami Yoshimoto,* Shinji Takagi,† Yoko Umemura,† Masahiko Hada,† and Hiroshi Nakatsuji†,‡

*Department of Applied Chemistry, Kyoto Prefectural University, Shimogamohanki-cho, Sakyo-ku, Kyoto 606, Japan; †Department of Synthetic Chemistry and Biological Chemistry, Faculty of Engineering, Kyoto University, Sakyo-ku, Kyoto 606-01, Japan; and ‡Institute of Fundamental Chemistry, Nishihiraki-cho, Sakyo-ku, Kyoto 606, Japan

Received October 8, 1996; revised August 28, 1997; accepted August 26, 1997

**The mechanism of the decomposition of formic acid HCOOH on ZnO(10$\bar{1}$0) surfaces was investigated using the *ab initio* molecular orbital method. Furthermore, the role of the dynamic bending of the surface formate anion $HCOO^-$ in the decomposition reaction was also examined. The lattice Zn atom interacts with the C–H bond of the adsorbed formate anion and cleaves the C–H bond to yield adsorbed $CO_2$ and ZnH species. However, similar results are not obtained with the lattice O atom or surface OH species. The energy barriers of C–H bond cleavage and $CO_2$ desorption from the surface were calculated to be 45.5 and 11.2 kcal/mol, respectively, at the MP2 level. $H_2$ formation is a bimolecular process: another formic acid from the gas phase attacks the ZnH surface species and produces an $H_2$ molecule. The calculated energy barrier is 2.2 kcal/mol and the exothermicity of the reaction is 11.3 kcal/mol at the MP2 level. These results indicate that the rate-determining step of the dehydrogenation decomposition of formic acid is cleavage of the C–H bond. Both the decomposition reaction and the dissociative adsorption of HCOOH occur more easily on hydrogen-covered surface than on a clean surface.** 

## 1. INTRODUCTION

Metal oxides play important roles in many catalytic processes (1–23). For example, zinc oxide is a major component of commercially available Cu/ZnO catalysts for methanol synthesis. Many studies have examined the decomposition processes associated with methanol, formaldehyde, and formic acid on ZnO surfaces (1–6). In the present study, we examined the decomposition of formic acid on a ZnO(10$\bar{1}$0) surface from a quantum-chemical perspective.

In water gas shift reactions on the surfaces of various metal oxides (12–15), such as MgO, $Al_2O_3$, and ZnO, the formate anion has been postulated to be a key intermediate. Formic acid is dissociatively adsorbed on metal and metal oxide surfaces at room temperature, and yields a formate anion and surface hydroxyl species (4–6, 10, 17–23). Three structures have been proposed for a formate anion that has adsorbed on metal oxide surfaces (4–6, 10, 17–23): bridging, bidentate, and unidentate, as shown in Fig. 1. Formic acid adsorbed on metal and metal oxide surfaces decomposes into $H_2O + CO$ or $H_2 + CO_2$ (1–6, 11–23). Many studies have attempted to clarify the active species, reactivities, and selectivities of the catalysts in the decomposition reaction of formic acid. Dehydrogenation, which is the decomposition of formic acid into $H_2 + CO_2$, occurs selectively on a ZnO surface (3). Dehydration, which produces $H_2O + CO$, occurs selectively on a MgO(001) surface (11).

The nature of the active sites, the structures of adsorbed species, and the mechanism of the surface reaction remain unclear. Theoretical studies have been performed to clarify the mechanisms of hydrogen chemisorption on ZnO (24, 25) and other metal oxide surfaces (26–33) and of the adsorption of formic acid on metal (16) and bimetal surfaces (34).

The decomposition reaction of formic acid in the gas phase has been studied theoretically, and the structures of the transition state and the activation energies for the dehydrogenation and dehydration reactions have been reported, as shown in Fig. 2 (35, 36). The mechanisms of the reactions on metal and metal oxide surfaces are expected to be different from those in the gas phase.

Previously, we performed theoretical studies of the adsorption of formic acid on MgO(001) (37) and ZnO(10$\bar{1}$0) (38, 39) surfaces. We used the $Zn_4O_4$ cluster embedded in an electrostatic potential to simulate the ZnO(10$\bar{1}$0) surface and described how formic acid is dissociatively adsorbed to form the formate anion and surface OH species with a small energy barrier (38). The favorable structures of the formate anion were considered to be a bridging or unidentate structure. The unidentate structure was stable because of interaction with the surface OH species, and the structure was more similar to molecularly-adsorbed HCOOH than to adsorbed $HCOO^-$. In the temperature range of the decomposition reaction, formic acid is dissociatively adsorbed into the formate anion and surface OH species on ZnO surfaces (3–5). Therefore, we adopt adsorbed bridging formate and surface OH species as an initial structure, as shown in Fig. 3.

When HCOOH is no longer supplied to the system, the formation of $CO_2$ continues, while the evolution of $H_2$ stops.



0021-9517/98 $25.00

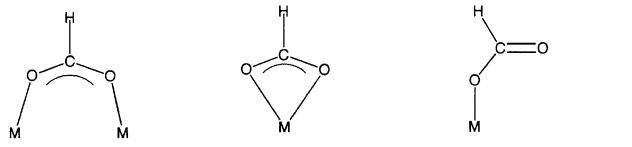


FIG. 1. Three possible geometries of formate anion on a metal oxide surface.

Noto *et al.* (3) suggested a mechanism for $H_2$ formation in which the formic acid molecule attacks the surface Zn–H species from the gas phase. Therefore, we investigated unimolecular $CO_2$ formation and both unimolecular and bimolecular $H_2$ formation. We assumed that $CO_2$ is produced by the decomposition of surface formate species, leaving adsorbed ZnH species. $CO_2$ formation requires only one HCOOH molecule, since the surface formate anion, which decomposes into $CO_2$ and surface OH species, is produced by the dissociative adsorption of HCOOH. We assume two mechanisms for $H_2$ formation:

1. $H_2$ molecules are formed by the reaction of two H atoms adsorbed on the ZnO surface.
2. A second HCOOH molecule attacks the adsorbed H atom to yield an $H_2$ molecule and adsorbed $HCOO^-$.

Path 1 is unimolecular regarding the reactant, since the two H atoms originate from a single HCOOH molecule. Since two HCOOH molecules are involved in path 2, it is bimolecular. The ZnH species is formed from the surface $HCOO^-$ by $CO_2$ formation, and the HCOOH comes from the gas phase in path 2.

We report our model for the ZnO($10\bar{1}0$) surface and the calculational method in Section 2. The contribution of the dynamic bending mode (23) of surface formate to the decomposition reaction and the mechanism of the $CO_2$ formation are reported in Sections 3 and 4, respectively. Two mechanisms of $H_2$ formation, i.e., unimolecular and bimolecular reactions, are discussed in Sections 5 and 6, respectively. The differences between the surface reaction on a clean surface and that on a hydrogen-covered surface are also discussed in Section 6. The results including electron correlation are discussed in Section 7.

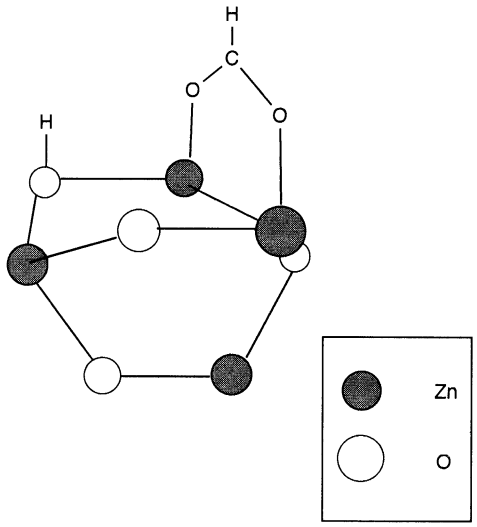


FIG. 3. Geometry of adsorbed $HCOO^-$ and OH species.

## 2. MODEL AND CALCULATIONAL METHOD

The crystal structure of ZnO is the Wurtzite structure shown in Fig. 4. We use the $Zn_4O_4$ cluster, which is shown in Fig. 5, embedded in an electrostatic field to simulate the Madelung potential. The $Zn_4O_4$ cluster includes the first, second, and third layers. The cluster is small and includes only two of the three nearest neighbors of the reaction sites. This small size may lead to greater reactivity than the actual surfaces, although we believe that our previous results are at least qualitatively correct. The Madelung potential is proportional to the ionic charge, $q$, in $Zn^{+q_4}O^{-q_4}$. There are several ways to estimate this quantity, but the results vary widely; e.g., $q \sim 1$ (40), $q \sim 0.8$ (41), and $q \sim 0.4$ (42). We

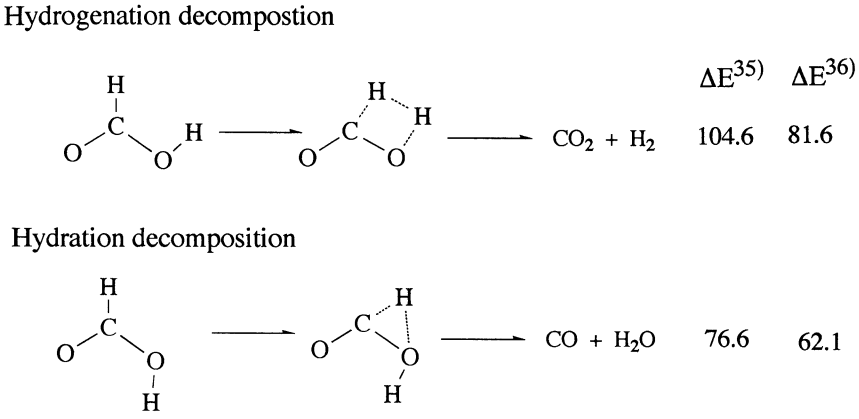


FIG. 2. Mechanism and energy barrier of the decomposition of HCOOH in the gas phase (35, 36). Energy barriers are expressed as kcal/mol.

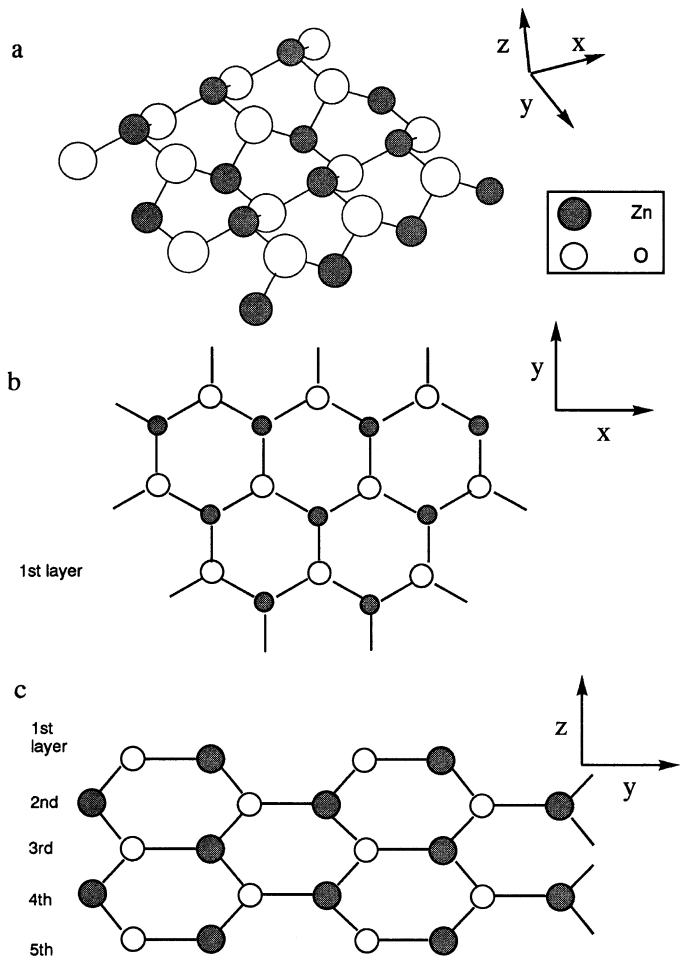


FIG. 4. Structure of a Wurtzite ZnO crystal lattice: (a) whole view of ZnO Wurtzite crystal lattice; (b) top view of ZnO(10$\bar{1}$0) surface; (c) side view of ZnO Wurtzite crystal lattice.

used $q = \pm 0.5$ for the point charges in the study of $H_2$ adsorption on a ZnO(10$\bar{1}$0) surface (24). We used a $q$ smaller than the calculated Mulliken atomic charge of a ZnO cluster because the electron density is spread out over the atomic region. Mulliken atomic charge of a $Zn_4O_4$ cluster calculated at the Hartree–Fock level is approximately $\pm 1.0$ on each atom in the present study. However, we used a smaller value, $q = \pm 0.5$, for the point charges from our previous experience (24). We placed the point charges, $+0.5$ on Zn and $-0.5$ on O, at 464 lattice sites around the $Zn_4O_4$ cluster. The first and second layers of the ZnO crystal shown in Fig. 2 are expressed by $Zn_{60}O_{60}$, and the third and fourth layers are expressed by $Zn_{56}O_{56}$. The whole ZnO model used in the present study has eight layers. The $Zn_4O_4$ cluster is located at the center of the surface.

The cluster geometry is fixed at the crystal lattice position with a ZnO distance of 1.95 Å during the surface reaction processes. Relaxation of the ZnO surface is expected to influence adsorption, but the large number of degrees of freedom represents a formidable optimization problem when they are included in the reaction path calculations. To avoid this problem, relaxation of the ZnO surface was not included in the calculation. Only the geometries of the adsorbates were optimized using the energy gradient method.

We use the $Zn_2O_2$ part of the first layer as the reaction site for the adsorption and dissociation of formic acid. For example, the bridging and bidentate formic acids are assumed to be adsorbed on Zn atoms as indicated by the arrows in Fig. 5. The molecular plane of the adsorbed formate species on metal and metal oxide surfaces has been reported to be perpendicular to the surface (10, 23, 43). Therefore, the molecular plane of the adsorbed formic anion was fixed perpendicular to the surface, except when noted otherwise.

The basis set used for the Zn atom is the (3*s*2*p*5*d*)/[2*s*2*p*2*d*] set of Hay and Wadt with the Ar core replaced by the effective core potential (44). The (9*s*5*p*)/[4*s*2*p*] sets of Huzinaga and Dunning are used for C and O atoms, while the (4*s*)/[2*p*] set is used for the H atom (45, 46). Hartree–Fock and MP2 calculations were carried out using the HONDO7 program (47).

## 3. CONTRIBUTION OF THE DYNAMIC BENDING MODE

The dynamic bending mode of the adsorbed formate anion, in which it tilts toward the surface, was observed on an Ag surface (23). Since the C–H bond interacts more effectively with the surface by tilting of the molecular plane,

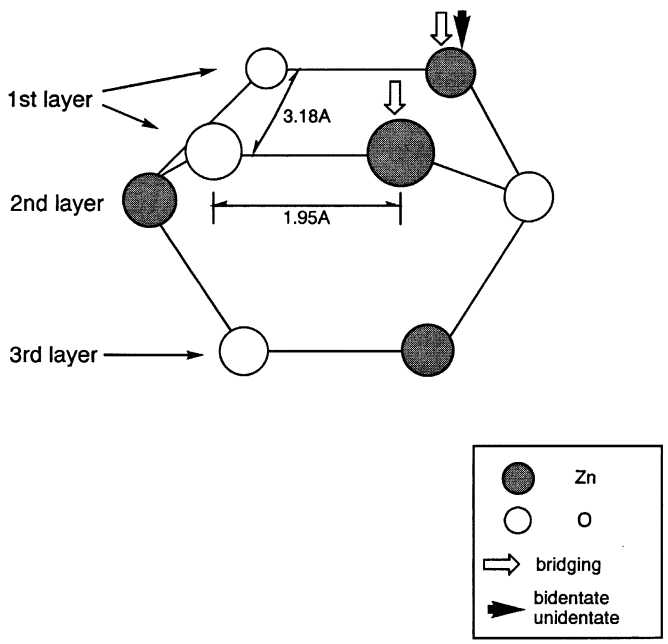


FIG. 5. $Zn_4O_4$ cluster as a model of a ZnO(10$\bar{1}$0) surface. This cluster is taken from the first, second, and third layers of a ZnO crystal lattice and placed in the electrostatic field presented by 464 point charges located on a ZnO crystal lattice. $Zn_4O_4$ of the first layer is used for adsorption and dissociation of HCOOH. Arrows indicate sites of formate adsorption in the bridging and bidentate forms.

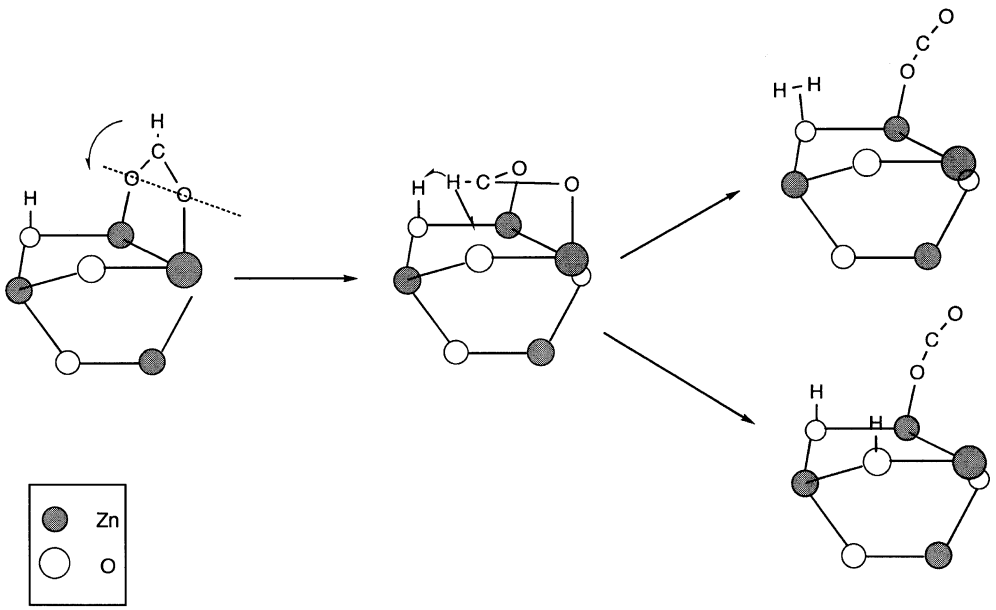


FIG. 6. Assumed decomposition path for bridging-type $HCOO^-$. Black and white circles represent the Zn and O lattice atoms, respectively.

this mode is expected to influence C–H bond cleavage (34). We examined this mode on MgO(001) (37) and ZnO(10$\bar{1}$0) (38) surfaces and found that the formate anion tilts easily as a result of a secondary perturbation: tilting the molecular plane by 90° requires only 19 kcal/mol.

We assume that decomposition has two steps, as shown in Fig. 6. In the first step, the molecular plane of the adsorbed formate anion tilts by approximately 90°. In the second step, the C–H bond is assumed to be cleaved by the lattice O atom, giving the surface OH species, or by the surface OH species, giving an $H_2$ molecule. As the molecular plane tilts, the two oxygen atoms of the formate anion are fixed onto the two lattice Zn atoms. However, both mechanisms involve energy barriers higher than 75 kcal/mol, which are too high to allow for the decomposition of the surface formate species.

We next examined how the bridging formate anion transforms into a bidentate structure and then tilts toward the surface. First we examined the dynamic bending mode of bidentate-type $HCOO^-$ on a ZnO surface. When $HCOO^-$ tilts up to $Q = 90$, the structure is unstable. The $p$ orbital of $HCOO^-$ interacts with the $s$ orbital of Zn atom; however, the $p$ orbital of the $HCOO^-$ has a node, as shown in Fig. 7, and decomposition of bidentate $HCOO^-$ does not seem to occur.

Based on these results, the dynamic bending mode does not appear to contribute to the decomposition reaction.

## 4. DECOMPOSITION REACTION FROM THE INTERMEDIATE

Since the interaction between the O atom of the adsorbed formate and the lattice Zn atom is relatively weak, cleavage of the O–Zn bond is expected to take place easily. Rotation around the C–O bond follows O–Zn bond cleavage and yields an intermediate product. Four structures of the intermediate are assumed, as shown by **a**, **b**, **c**, and **d** in Fig. 8. The C–H bond interacts with the lattice Zn atom in structures **a** and **b**. The C–H bond interacts with the Zn atom in the same Zn–O unit as the surface OH species in structure **a**. In structure **b**, the Zn–O unit is different from that of the surface OH species. The C–H bond interacts with the lattice O atom and surface OH species in structures **c** and **d**. However, since structures **c** and **d** are unstable, the discussion of geometry optimization will not include these structures.

When cleavage of the C–H bond starts from structures **a** and **b**, structures **e** and **f**, respectively, are expected to be the products. A $CO_2$ molecule is desorbed from the surface, and the two adsorbed H atoms remain on the surface. We investigated the geometry of the ZnH and OH species after the desorption of $CO_2$. The optimized geometries and the Mulliken populations are shown in Fig. 9. The H atom is

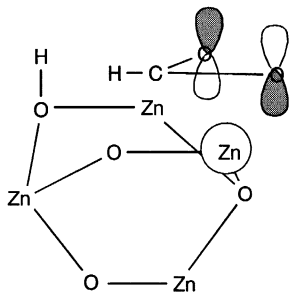


FIG. 7. Overlap between the $p\pi^*$ orbital of bidentate formate anion and the $s$ orbital of lattice Zn atom.

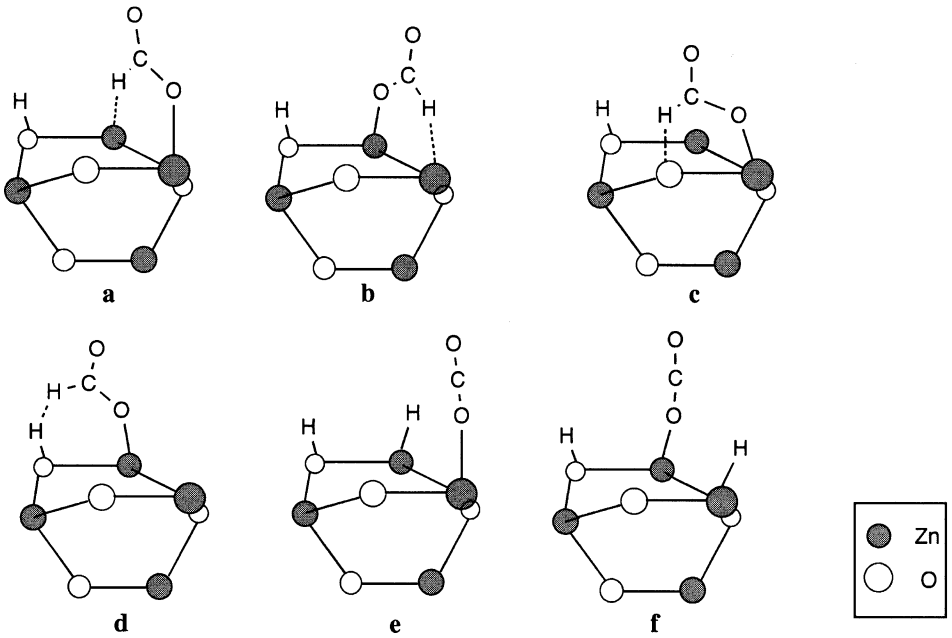


FIG. 8. Assumed structures of unidentate-like $HCOO^-$ and products. Structures **a**, **b**, **c**, and **d** show unidentate-like $HCOO^-$ and surface OH species, while structures **e** and **f** show adsorbed $CO_2$, ZnH and OH species.

adsorbed at the same Zn–O unit as the surface OH species in structure **g**, while it is adsorbed on a different Zn–O unit in structure **h**. Structure **g** is 38.3 kcal/mol more stable than structure **h**. Furthermore, the OH and ZnH species appear to influence each other through the Zn–O bond. We previously reported surface activation by the adsorbed formate anion, where the 2 $p_z$ orbital of the lattice O atom located next to the adsorption site is activated by the adsorbed formate anion (37, 38). We believe that the atom directly bonded to the active site is also activated in this case.

Next, the geometries of structures **e**, **f** and the transition states (TS1, TS1′) are fully optimized. TS1 and TS1′ are the transition states in the reactions from structure **a** to **e** and from structure **b** to **f**, respectively. The molecular plane composed of the O and H atoms of the formate anion and the two lattice Zn atoms is assumed to be perpendicular to the surface during optimization of the transition states. The optimized geometries of structures **e** and TS1 are almost the same as those of structure **f** and TS1′, respectively. The optimized geometries and Mulliken populations of the bridging-type formate species, transition state (TS1), and structure **e** are shown in Fig. 10. The C–O bond length of TS1 is shorter than that of the bridging structure and is close to that of $CO_2$. The Zn–H distance of TS1 is almost the same as that in the surface ZnH species, as shown in Fig. 9. The angle OCO of TS1 is wider than that of the

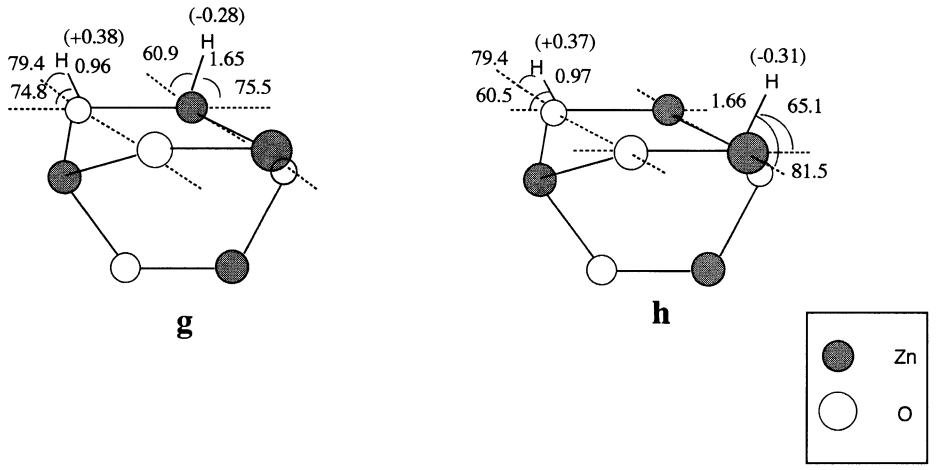


FIG. 9. Fully optimized geometric parameters of ZnH and OH species adsorbed on a ZnO surface. Bond distances and angles are expressed as Å and degrees, respectively. Values in parentheses show the net atomic charge.

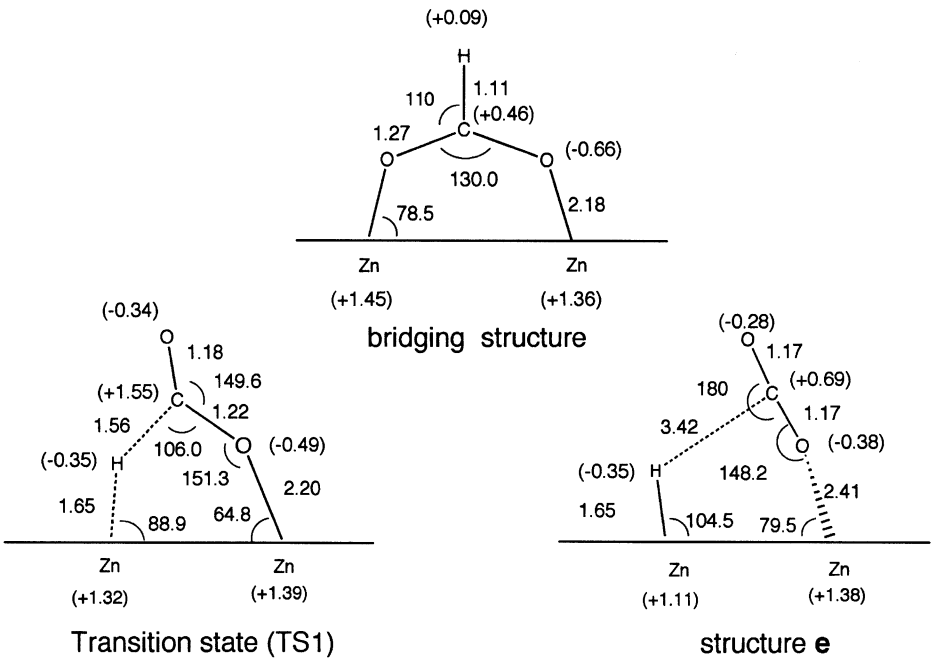


**FIG. 10.** Fully optimized geometric parameters of bridging-type $HCOO^-$, transition state (TS1), and structure **e** (Fig. 6) on a ZnO surface. Bond distances and angles are expressed as Å and degrees, respectively. Values in parentheses show the net atomic charge.

bridging structure. We have assumed that $CO_2$ is adsorbed on the surface after decomposition. However, desorption from the surface may occur directly without adsorption.

Figure 11 shows the energy profile, where $\Delta E$ is defined by

$$\Delta E = E - E \text{ (initial structure)}. \quad [1]$$

The initial structure is shown in Fig. 3. TS1 is 39.6 kcal/mol more stable than TS1′, and structure **e** is 38.3 kcal/mol more stable than structure **f**. Therefore, the decomposition reaction from structure **a** to **e** is more favorable than that from structure **b** to **f**. The net charge on the Zn atom located at the same Zn–O unit as the OH species is +1.45 on the bridging structure shown in Fig. 10, while that of another Zn atom is +1.36. The Zn atom at the same Zn–O unit as the OH species is more favorable as a hydrogen abstraction site from the C–H bond than is a Zn atom of another unit. The energy barrier from the bridging

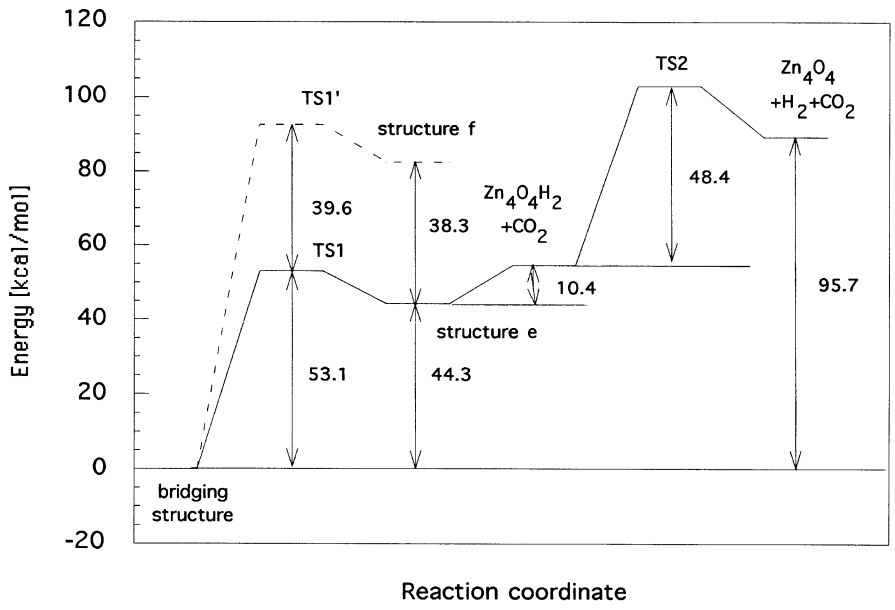


**FIG. 11.** Energy profile of the formation of $CO_2$ and unimolecular $H_2$ on a ZnO surface.

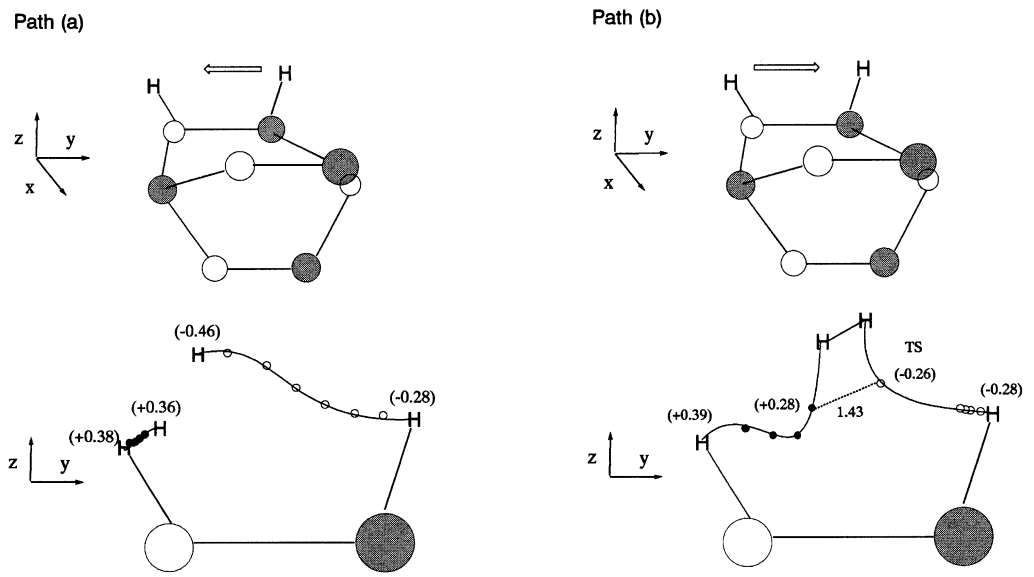


FIG. 12. Schematic representation of $H_2$ formation paths and fully optimized results. The lower figures represent the fully optimized $H_2$ formation paths. The H atom of ZnH species moves in path (a), and the H atom of OH species moves in path (b). TS denotes the geometry of the transition state in path (b). Black and white circles represent the Zn and O lattice atoms, respectively.

structure to structure **e** is relatively large, 53.1 kcal/mol. The reaction from the bridging structure to structure **e** is endothermic by 44.3 kcal/mol. The energy barrier for the desorption of $CO_2$ from the surface is 10.4 kcal/mol.

## 5. UNIMOLECULAR REACTION TO YIELD AN $H_2$ MOLECULE

We next assume two paths for the unimolecular reaction, as shown in Fig. 12. The H atom adsorbed on the Zn atom moves toward the surface OH species in path (a), while the H atom adsorbed on the lattice O atom moves toward the surface ZnH species in path (b). In path (a), the $H_2$ molecule is not formed. However, the $H_2$ molecule is formed with an energy barrier of 48.4 kcal/mol in path (b). The reaction route of the H atoms in path (b) is almost the same as that in the dissociative adsorption of an $H_2$ molecule on a ZnO(10$\bar{1}$0) surface. Although path (b) is more favorable than path (a), the overall reaction is endothermic by 95.7 kcal/mol, as shown in Fig. 11.

## 6. BIMOLECULAR REACTION TO FORM AN $H_2$ MOLECULE

We assume in the bimolecular reaction that another free formic acid in the gas phase attacks the hydrogen atoms adsorbed on the surface. *Trans*-formic acid is only 6.4 kcal/mol more stable than *cis*-formic acid in the gas phase (38). Therefore, we examined whether both *trans*- and *cis*-formic acids attack the surface.

Figure 13 shows the assumed reaction pathway for *cis*-formic acid. *Cis*-formic acid approaches from the gas phase,

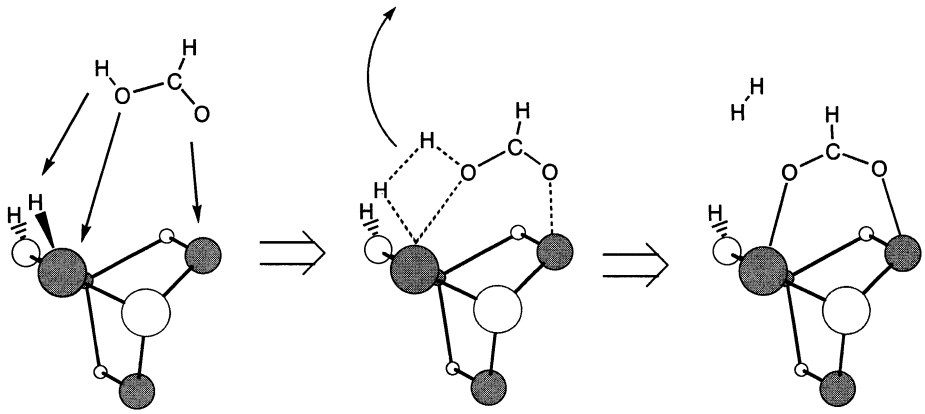

FIG. 13. Assumed $H_2$ formation path. *Cis*-formic acid attacks H adsorbed on a ZnO surface giving a bridging formate anion and an $H_2$ molecule. Black and white circles represent the Zn and O lattice atoms, respectively.

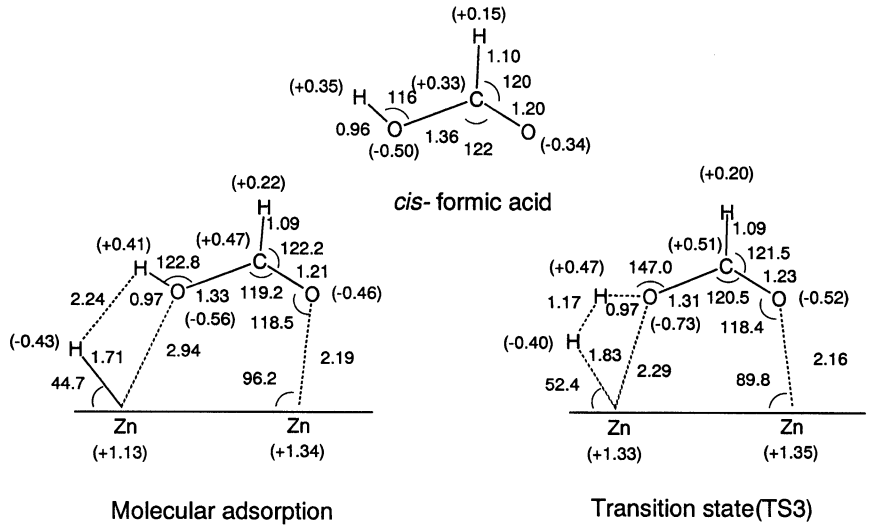


FIG. 14. Fully optimized geometric parameters for free *cis*-HCOOH, molecular adsorption state, and transition state (TS3) shown in Fig. 13. Bond distances and angles are expressed as Å and degrees, respectively. Values in parentheses show the net atomic charge.

allowing the two O atoms to interact with the two lattice Zn atoms and allowing the acidic H atom to interact with the H atom adsorbed on the Zn atom. This H atom interacts repulsively with the H atom adsorbed on the O atom. O–H bond cleavage and $H_2$ formation follow the molecular adsorption of *cis*-HCOOH. The optimized geometries and Mulliken populations for *cis*-formic acid, the molecular adsorption state, and the transition state (TS3) are shown in Fig. 14. The four-membered ring, composed of the two H atoms, the O, and the lattice Zn atom, is formed in the transition state. The energy barrier for TS3 to form the bridging formate and $H_2$ molecule is 6.7 kcal/mol, and the overall reaction is endothermic by 10.1 kcal/mol. The energy profile of the whole reaction is shown in Fig. 15.

Next, the path for *trans*-formic acid was determined as shown in Fig. 16. Only the carbonyl O atom interacts with the lattice Zn atom, and the protic H atom interacts with the H that is adsorbed on the Zn atom. The other O atom of HCOOH does not interact with the lattice atoms. Despite optimization of the transition state, the structure was

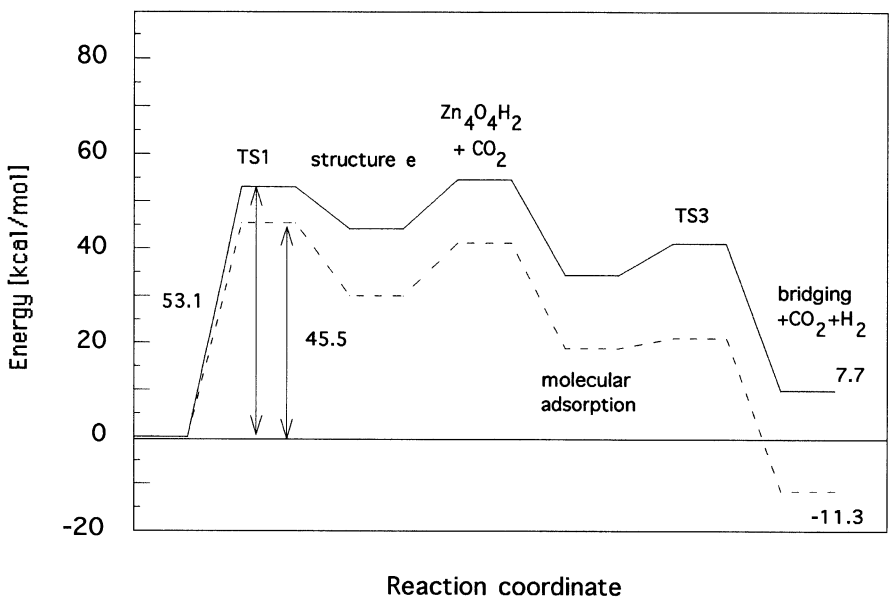


FIG. 15. Energy profile of $CO_2$ formation and bimolecular $H_2$ formation on a ZnO surface. Solid and broken lines denote energies calculated at the HF and MP2 levels, respectively.

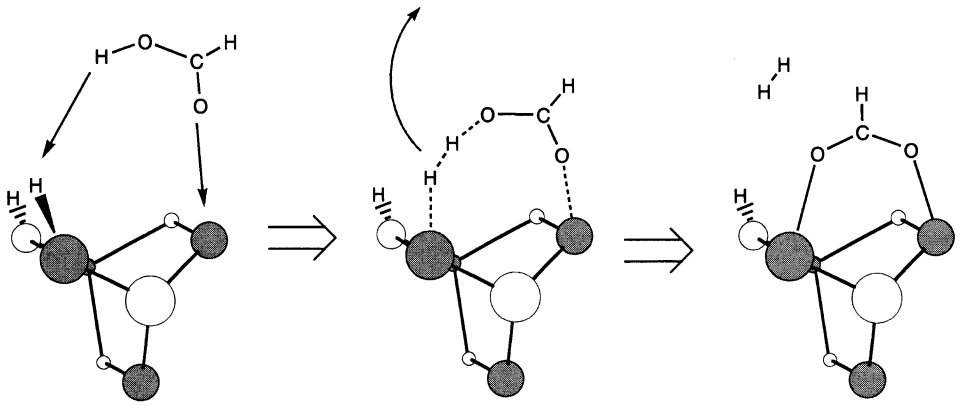

FIG. 16. Assumed $H_2$ formation path. *Trans*-formic acid attacks H adsorbed on a ZnO surface to form bridging formate anion and an $H_2$ molecule. Black and white circles represent the Zn and O lattice atoms, respectively.

found to be unstable. This structure of $HCOO^-$ is almost the same as that of the unidentate formate anion which does not interact with the ZnO surface, as reported previously (38). Therefore, we concluded that *trans*-HCOOH is not involved in the bimolecular decomposition reaction.

In summary, the formation of $H_2$ and $CO_2$ from formate adsorbed on a ZnO surface occurs by the following three steps:

$$Zn(l) + HCOO(a) \rightarrow ZnH(a) + CO_2(a) \quad [2]$$

$$CO_2(a) \rightarrow CO_2(g) \quad [3]$$

$$ZnH(a) + HCOOH(g) \rightarrow Zn(l) + HCOO(a) + H_2(g). \quad [4]$$

The rate-determining step is step (2), in which the C–H bond is cleaved to form $CO_2$.

Noto *et al.* (3) studied the decomposition of formic acid using adsorption measurements and an infra-red technique on a ZnO surface. When formic acid was trapped out of the system, the evolution of hydrogen stopped, while that of carbon dioxide continued at the same rate. Based on these results, they suggested the following mechanism:

1. The evolution of carbon dioxide arises from the decomposition of a formate anion, while the hydrogen atom remains on the surface.
2. The formic acid molecules attack the adsorbed hydrogen atoms, and surface formate anions and hydrogen atoms are formed.

The present theoretical results support the mechanism they suggested.

The present results indicate a difference between the dissociative adsorption of HCOOH on clean and on hydrogen-covered surfaces. The energy barrier of dissociative adsorption on a clean surface was 11.7 kcal/mol (38), while that on a hydrogen-covered surface was 6.7 kcal/mol. Thus, a hydrogen-covered surface is more reactive than a clean surface for this kind of surface reaction.

## 7. EFFECT OF ELECTRON CORRELATION

We examined the effect of electron correlation on the decomposition path using the MP2 method. The results are shown in Table 1 and Fig. 15, in which the geometries optimized at the HF level are used. In Fig. 15, the overall features of the reaction diagram are similar for the HF and MP2 results. However, upon closer examination, we note several differences. The energy barriers at the MP2 level are smaller than those at the HF level. Molecular adsorption is more stable at the MP2 level than at the HF level. The overall reaction is endothermic at the HF level, whereas electron correlation reveals that the reaction is exothermic by 11.3 kcal/mol. Ueno *et al.* reported an activation energy of 37.9 kcal/mol for the formate decomposition reaction on ZnO powders (15), and Vohs and Barteau reported an

TABLE 1

**The Energy Barriers ($\Delta E^{\ddagger}$) and Formation Energies ($\Delta E$) Calculated at the HF and MP2 Levels**

| | HF | MP2 |
|---|---|---|
| $\Delta E^{\ddagger}$ (TS1)[a] | 53.1 | 45.5 |
| $\Delta E$ ($CO_2$ desorption)[b] | 10.4 | 11.2 |
| $\Delta E$ (molecular adsorption)[c] | 31.7 | 19.0 |
| $\Delta E^{\ddagger}$ (TS3)[d] | 6.7 | 2.2 |
| $\Delta E$ (bridging structure + $CO_2$ + $H_2$)[e] | 7.7 | −11.3 |

[a] Energy barrier of Eq. [2] in Section 6.
[b] Energy barrier of Eq. [3] in Section 6.
[c] Energy difference between the initial structure and molecular adsorption shown in Fig. 14. Energy difference is calculated by Eq. [1].
[d] Energy barrier of Eq. [4] in Section 6.
[e] Energy difference between the initial structure and products. Energy difference is calculated by Eq. [1].

activation energy of 35.8 kcal/mol on a Zn-polar surface (1): activation energies on nonpolar and polar Zn surfaces are almost the same. This result is supported by the present result that only Zn atoms serve as reaction sites in the decomposition reaction of formic acid. The activation energy for the decomposition reaction is 45.5 and 53.1 kcal/mol at the MP2 and HF levels, respectively, and therefore the MP2 result is more reasonable than the HF result, in view of the experimental data.

## 8. SUMMARY

The results of the present theoretical study on the decomposition of formic acid on a ZnO($10\bar{1}0$) surface can be summarized as follows:

(1) Cleavage of the C–H bond does not appear to occur on the lattice O atom or on the surface OH species, while it does occur on the Zn atom through a unidentate-like intermediate with an energy barrier of about 45 kcal/mol (MP2 level).

(2) Although we expected that dynamic bending of the surface formate anion on a ZnO($10\bar{1}0$) surface would play an important role, we did not obtain any clear results which would support this view.

(3) The energy barrier for the unimolecular $H_2$ formation reaction was calculated to be 48.4 kcal/mol at the HF level, and the overall HCOOH decomposition reaction on a ZnO surface was determined to be endothermic. In contrast, the energy barrier of the bimolecular $H_2$ formation reaction was 6.7 kcal/mol at the HF level and 2.2 kcal/mol at the MP2 level, and the overall HCOOH decomposition reaction on a ZnO surface was exothermic by 11.3 kcal/mol at the MP2 level.

(4) We concluded that $CO_2$ formation is due to a unimolecular reaction, whereas $H_2$ formation is due to a bimolecular reaction. The rate-determining step lies in the $CO_2$ formation step through cleavage of the C–H bond. Only the Zn atom serves as a reaction site in this decomposition reaction.

(5) The energy barrier for dissociative adsorption on a clean surface was 7.5 kcal/mol at the MP2 level (38), while that on a hydrogen-covered surface was 2.2 kcal/mol at the MP2 level. Thus, the dissociative adsorption of HCOOH on a hydrogen-covered surface is preferable to that on a clean surface.

## ACKNOWLEDGMENTS

We thank the IMS Computer Center for allowing us to use their computer facilities to carry out the calculations. This study was supported in part by the New Energy and Industrial Technology Department Organization (NEDO) and by a Grant-in-Aid for Scientific Research from the Ministry of Education, Science and Culture.

## REFERENCES

1. Vohs, J. M., and Barteau, M. A., *Surf. Sci.* **176**, 91 (1986).
2. Lüth, H., Rubloff, G. W., and Grobman, W. D., *Solid State Comm.* **18**, 1427 (1976).
3. Noto, Y., Fukuda, K., Onish, T., and Tamaru, K., *Trans. Faraday Soc.* **63**, 3081 (1967).
4. Au, C. T., Hirsch, W., and Hirschwald, W., *Surf. Sci.* **199**, 507 (1988).
5. Petrie, W. T., and Vohs, J. M., *Surf. Sci.* **245**, 315 (1991).
6. Akhter, S., Cheng, W. H., Lui, K., and Kung, H. H., *J. Catal.* **85**, 437 (1984).
7. Foyt, D. C., and White, J. M., *J. Catal.* **47**, 260 (1977).
8. (a) Liang, S. H. C., and Gay, I. D., *J. Catal.* **101**, 193 (1986); (b) Takezawa, N., Hanamaki, C., and Kobayashi, H., *J. Catal.* **38**, 101 (1975).
9. Kagel, R. O., and Greenler, R. G., *J. Chem. Phys.* **49**, 1638 (1968).
10. Yamamoto, H., Akamatsu, N., Wada, A., Domen, K., and Hirose, C., *J. Electr. Spectrosc. Rel. Phenomena* **64/65**, 507 (1993).
11. Domen, K., Akamatsu, N., Yamamoto, H., Wada, A., and Hirose, C., *Surf. Sci.* **283**, 468 (1993).
12. Shido, T., Asakura, K., and Iwasawa, Y., *J. Catal.* **122**, 55 (1990).
13. Meschter, P. J., and Grabke, H., *J. Metal Trans. B* **10**, 323 (1979).
14. Sato, S., and White, J. M., *J. Am. Chem. Soc.* **102**, 7209 (1980).
15. Ueno, A., Onishi, T., and Tamaru, K., *Trans. Faraday Soc.* **67**, 3585 (1971).
16. Tanaka, S., Onchi, M., and Nishijima, M., *J. Chem. Phys.* **91**, 2712 (1989).
17. Ohnish, H., Egawa, C., Aruga, T., and Iwasawa, Y., *Surf. Sci.* **191**, 479 (1987).
18. Parrott, S. L., Rogers, J. W., Jr., and White, J. M., *Appl. Surf. Sci.* **1**, 443 (1978).
19. Bowker, M., Houghton, H., and Waugh, K. C., *J. Chem. Faraday Trans.* **77**, 3023 (1981).
20. Sun, Y. K., and Weiberg, W. H., *J. Chem. Phys.* **94**, 4587 (1991).
21. Solymosi, F., Kiss, J., Kovacs, I., *Surf. Sci.* **192**, 47 (1987).
22. Falconer, J. L., and Madix, R. J., *Surf. Sci.* **46**, 473 (1974).
23. Stevens, P. A., Madix, R. J., and Stohr, J., *Surf. Sci.* **230**, 1 (1990).
24. Nakatsuji, H., and Fukunishi, Y., *Int. J. Quantum. Chem.* **42**, 1101 (1992).
25. Anderson, A. B., and Nichols, J. A., *J. Am. Chem. Soc.* **108**, 4742 (1986).
26. Nakatsuji, H., Hada, M., Nagata, K., Ogawa, H., and Domen, K., *J. Phys. Chem.* **98**, 11840 (1994).
27. (a) Nakatsuji, H., and Hada, M., *J. Am. Chem. Soc.* **107**, 8264 (1985); (b) Nakatsuji, H., Hada, M., and Yonezawa, T., *J. Am. Chem. Soc.* **109**, 1902 (1987).
28. Nakatsuji, H., Matsuzaki, Y., and Yonezawa, T., *J. Chem. Phys.* **88**, 5759 (1988).
29. (a) Sawabe, K., Koga, N., and Morokuma, K., *J. Chem. Phys.* **97**, 6871 (1988); (b) Anchell, J. L., Morokuma, K., and Hess, A. C., *J. Chem. Phys.* **99**, 6004 (1993).
30. Kobayashi, H., Yamaguchi, M., and Ito, T., *J. Phys. Chem.* **94**, 7206 (1990).
31. Colbourn, E. A., and Mackrodt, W. C., *Surf. Sci.* **117**, 571 (1992).
32. Sauer, J., Kolmel, C. M., Hiller, J. R., and Ahlrichs, R., *Chem. Phys. Lett.* **164**, 193 (1989).
33. Sauer, J., *J. Phys. Chem.* **91**, 2315 (1987).
34. Pápai, I., Ushio, J., and Salahub, D. R., *Surf. Sci.* **282**, 262 (1993).
35. Yamashita, K., and Yamabe, T., *Int. Quantum Chem. Symp.* **17**, 117 (1983).
36. Saito, K., Kakumoto, T., Kuroda, H., Torii, S., and Imamura, A., *J. Chem. Phys.* **80**, 4989 (1984).
37. Nakatsuji, H., Yoshimoto, M., Hada, M., Domen, K., and Hirose, C., *Surf. Sci.* **336**, 232 (1995).

38. Nakatsuji, H., Yoshimoto, M., Umemura, Y., Takagi, S., and Hada, M., *J. Phys. Chem.* **100**, 694 (1996).
39. Zanpeisov, N. U., Nakatsuji, H., Hada, M., and Yoshimoto, M., *J. Mol. Catal.*, in press.
40. Heiland, G., Kurstman, P., and Pfister, H., *Z. Physik.* **176**, 485 (1963).
41. Harrison, W. A., *Phys. Rev. B* **10**, 767 (1974).
42. Phillips, J. C., *in* "Covalent Bonding in Crystals, Molecular and Polymers," Univ. of Chicago Press, Chicago, 1969.
43. Weisel, M. D., Chen, J. G., Hoffman, F. M., Sun, Y. K., and Weinberg, W. H., *J. Chem. Phys.* **97**, 9396 (1992).
44. Hay, P. J., and Wadt, W. R., *J. Chem. Phys.* **82**, 270 (1985).
45. Huzinaga, S., *J. Chem. Phys.* **42**, 1293 (1965).
46. Dunning, T. H., Jr., *J. Chem. Phys.* **53**, 2823 (1970).
47. King, H. F., Dupis, M., Villar, H., and Hurst, G. J. B., "Program Library HONDO7 (No. 1501)," The Computer Center of Institute for Molecular Science, Okazaki, Japan, 1989.